ADVANCED MATERIALS
www.advmat.de

Atomic Spatial and Temporal Imaging of Local Structures and Light Elements inside Zeolite Frameworks

Boyuan Shen, Xiao Chen, Dali Cai, Hao Xiong, Xin Liu, Changgong Meng, Yu Han, and Fei Wei**

Identifying the atomic structures of porous materials in spatial and temporal dimensions by (scanning) transmission electron microscope ((S)TEM) is significant for their wide applications in catalysis, separation and energy storage. However, the sensitivity of materials to electron beams made it difficult to reduce the electron damage to specimens while maintaining the resolution and signal-to-noise ratio. It is therefore still challenging to capture multiple images of the same area in one crystal to image the temporal changes of lattices. Usings integrated differential phase contrast (iDPC) STEM, atomic-resolution imaging of beam-sensitive zeolite frameworks is achieved with an ultralow dose of 40 e^{-} $Å^{-2}$, 2–3 orders of magnitude lower than that of conventional STEM. Based on the iDPC technique, not only the atomic 3D architecture of ZSM-5 crystals but also the changes of frameworks are observed during in situ experiments. Local structures and light-element aromatics in ZSM-5 crystals can also be revealed directly under iDPC-STEM. These results provided not only an efficient tool to image beam-sensitive materials with ultralow beam current but also a new strategy to observe and investigate the hydrocarbon pools in zeolite catalysts at the single-molecule scale.

Porous materials, including metal–organic, covalent-organic, and zeolite frameworks, have shown great application potential in catalysis, separation, and energy storage due to their unique channel geometry and high surface-volume ratio.[1–7] Zeolites are a class of the earliest porous materials to be widely studied and applied in both laboratory and industry.[5–7] Using different synthesis methods, diverse zeolite frameworks with tunable channel systems were designed and established. ZSM-5 (MFI type) is one of the most studied inorganic zeolites, since its structure was first revealed in 1978.[8,9] The ZSM-5 framework owns a unique cross-linked channel system with the straight channels (5.6 Å × 5.3 Å) along *b*-axis and the sinusoidal channels (5.5 Å × 5.1 Å) along *a*-axis (**Figure 1**a). The ZSM-5 catalysts exhibit excellent shape selectivity and were efficiently used in many aromatization reactions due to their perfectly matched channel size with the aromatics (known as hydrocarbon pools).[10–14] And the channel geometry and flexibility will strongly influence the sorption and diffusion of small molecules in the hydrocarbon pools.[15–19] Thus, revealing the atomic structure of ZSM-5 framework is of great significance to promote its further applications in diverse science and engineering disciplines.

The diffraction methods were used to reveal the accurate periodic crystalline structures and helped us to understand the architectures of various porous frameworks, including the MFI-type frameworks.[8,9,20–22] However, since the diffraction methods only provided the average results over bulk materials, our understandings on the local structures of ZSM-5 crystals are still insufficient, including the interfaces, defects and surface terminations, which strongly influence the tailored functions of nanomaterials. Thus, the imaging technique was rapidly developed to achieve the real-space observations of such local structures. The obtained images of 2D projections from different directions described the 3D structures of regularly shaped crystals in the real space. Moreover, the development of in situ techniques helped us to study the changes of lattice structures with additional temporal dimension.

The (scanning) transmission electron microscope ((S)TEM) is one of the most powerful imaging tools for the atomic-resolution

B. Shen, Dr. X. Chen, D. Cai, H. Xiong, Prof. F. Wei
Beijing Key Laboratory of Green Chemical Reaction Engineering and Technology
Department of Chemical Engineering
Tsinghua University
Beijing 100084, China
E-mail: chenx123@tsinghua.edu.cn; wf-dce@tsinghua.edu.cn

Prof. X. Liu, Prof. C. Meng
School of Chemistry
Dalian University of Technique
Dalian 116024, China

Prof. X. Liu, Prof. Y. Han
KAUST Catalysis Center
Physical Sciences and Engineering Division
King Abdullah University of Science and Technology
Thuwal 23955-6900, Saudi Arabia

Prof. Y. Han
Advanced Membranes and Porous Materials Center
Physical Sciences and Engineering Division
King Abdullah University of Science and Technology
Thuwal 23955-6900, Saudi Arabia

The ORCID identification number(s) for the author(s) of this article can be found under https://doi.org/10.1002/adma.201906103.

DOI: 10.1002/adma.201906103

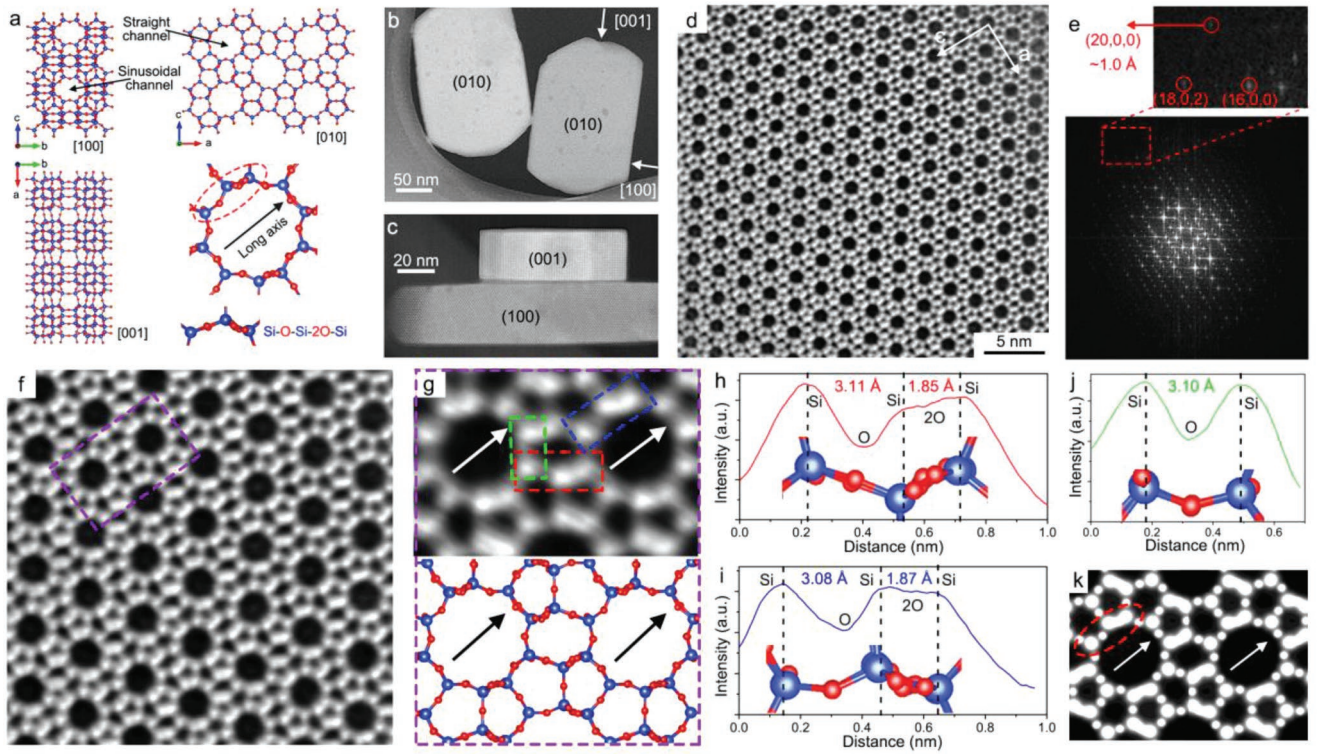

Figure 1. Atomic-resolution iDPC-STEM imaging of the [010] projection of ZSM-5. a) The structural model of ZSM-5 framework of different projections. b,c) The HAADF-STEM images of the short-*b*-axis ZSM-5 nanocrystals. b) It shows two planar ZSM-5 crystals with exposed (010) surfaces. The typical zone axes for 3D imaging are marked with white arrows. And c) shows two vertical ZSM-5 crystals with exposed (100) and (001) surfaces respectively. d,e) The iDPC-STEM image d) and corresponding FFT pattern e) of ZSM-5 from the [010] projection. The (20,0,0) plane indicates an information transfer of about 1 Å. f,g) The magnified iDPC-STEM images of ZSM-5 showing the atomic-resolution straight channels as the elliptical Si_{10}-rings. h–j) The profile analysis of three structural units on the framework marked as three colored frames in (g). The intensity profiles exhibit the contrasts and projected distances between different atoms. k) The integration mapping of the projected electrostatic potential in ZSM-5 framework from the [010] projection.

characterization of nanostructures and lattices.[23–25] However, the porous catalysts are always sensitive to the electron beams and cannot be imaged under a high electron dose in the (S)TEMs,[26–38] which limited the resulting resolution and signal-to-noise ratio. Recently, the emergent integrated differential phase contrast (iDPC) technique[39–42] allowed us to image the beam-sensitive materials with a high resolution and signal-to-noise ratio under an ultra-low beam current. The set-up of iDPC-STEM is shown in Figure S1 (Supporting Information). The iDPC-STEM enabled the linear imaging of the projected electrostatic potential in lattice, and the resulting contrast is nearly proportional to the atomic number Z instead of its square in the high angle annular dark field (HAADF) STEM, greatly improving the capacity of light-element imaging. And the lower damage allowed us to obtain continuous images of the same area so that we can investigate the temporal changes of structures as a 4D imaging especially in the in situ experiments. These advantages made the iDPC-STEM an efficient tool to study various porous catalysts and inside hydrocarbon pools.

In this work, we reduced the electron dose during the iDPC-STEM imaging lower than 40 e^{-} $Å^{-2}$ without any cost of reducing resolution (≈1 Å) and signal-to-noise ratio. Based on the iDPC-STEM, we unraveled the atomic-resolution 3D framework of the short-*b*-axis ZSM-5 crystals with clear surface terminations and interface structures. The iDPC-STEM images show the exact projected position of each atom, especially for the light elements. Such well-defined ZSM-5 framework provides an ideal platform to study the various behaviors of guest molecules. Due to negligible damage under such low beam current, we further achieved the real-space imaging of para-xylenes (PXs) confined in ZSM-5 framework directly under iDPC-STEM, and revealed the sorption behaviors of PXs at the single-molecule level.

The structural model of ZSM-5 framework is shown in Figure 1a. From the [010] projection, the straight channel formed by Si_{10}-rings can be directly identified. And based on the numbers of atoms in the projection, the Si-O-Si-2O-Si units around the channels are marked for further analysis by the STEM. Figure 1b shows the short-*b*-axis ZSM-5 crystals with near hexagonal projection viewed from the [010] direction by the STEM, and the corresponding zone axes are marked by the white arrows. These ZSM-5 nanocrystals were synthesized via a hydrothermal process[13,14] (see details in "Materials and Methods" section in the Supporting Information) and show a coffin shape with uniform thickness. The length of single nanocrystal is over 200 nm, while the thickness is limited to 30–50 nm (Figure S2, Supporting Information). The resulting smooth surface makes it easy to identify the different zone

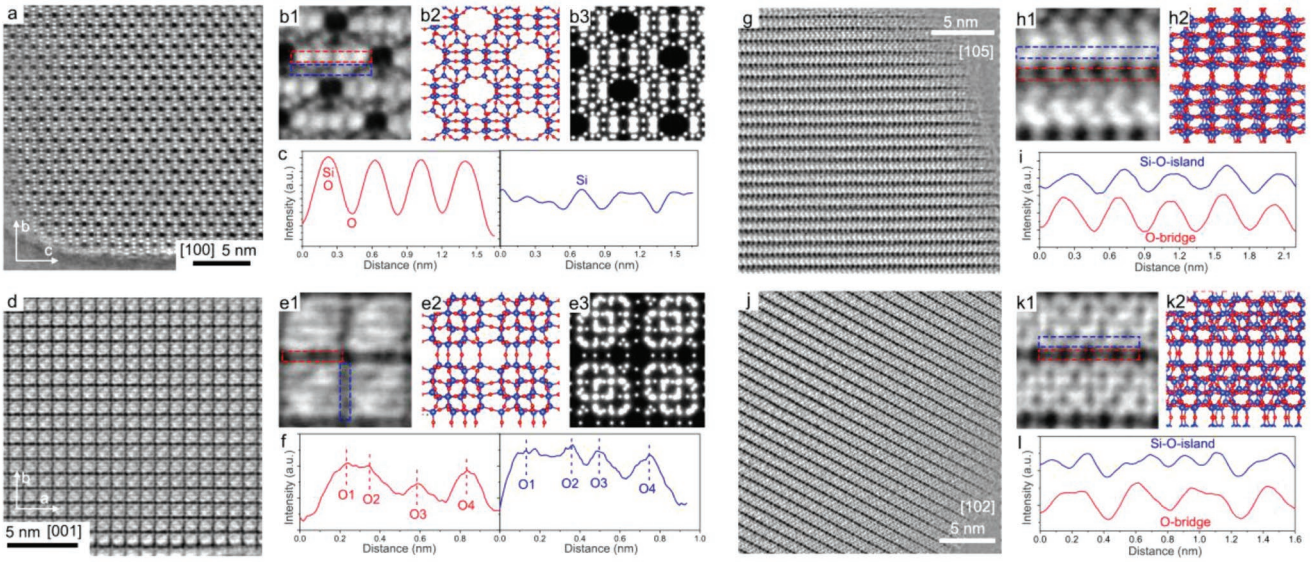

Figure 2. The 3D iDPC-STEM imaging of ZSM-5 framework. a–c) The iDPC-STEM image a) and detailed analysis b,c) from the [100] direction. The imaged structure is consistent with the structural model and calculated electrostatic potential (b). And the intensity profiles (c) show the detailed atomic position of each element. d–f) The iDPC-STEM image d) and detailed analysis e,f) from the [001] direction. Especially, the intensity profiles (f) show the capacity of iDPC-STEM for imaging light O bridges, where the positions of four O atoms are clearly marked. g–i) The iDPC-STEM image g) and detailed analysis h,i) from the [105] direction. j–l) The iDPC-STEM image j) and detailed analysis k,l) from the [102] direction. These two higher-index surfaces were found out to give a more obvious imaging of O bridges as shown in the profile analysis.

axes for a multiview imaging of 3D lattice structures. For example, the ZSM-5 crystals in Figure 1c exhibit two exposed crystal surfaces from the lateral view, including (100) and (001) as marked. From these lattice directions, we can obtain a 3D structural analysis of ZSM-5 framework revealing its detailed channel system and local structures.

In the previous studies on ZSM-5, the (010) surface is a characteristic plane with the visible straight channels consisting of Si_{10}-rings, which are of great significance of the adsorption and reaction in the hydrocarbon pools. Figure 1d shows the iDPC-STEM image of ZSM-5 (010) surface with the ordered straight channels. In the corresponding fast Fourier transform (FFT) pattern (Figure 1e), the (20,0,0) plane gives an information transfer of ≈1 Å indicating the highest resolution ever reported. Then, in the magnified iDPC-STEM images (Figure 1f,g), the clear positions of Si and O atoms are displayed and the Si_5- and Si_6- rings around the straight channels also can be identified. When compared to the annular dark field (ADF) and bright field (BF) STEM imaging, the iDPC technique provides obvious higher resolution and signal-to-noise ratio (Figure S3, Supporting Information) so that the exact positions of atoms can be identified directly under STEM. Especially, based on the different Si–Si distances in the [010] projection, the long-axis direction and Si-O-Si-2O-Si units were marked as the white arrows and dash-line frames in Figure 1g respectively.

Then, we used the profile analysis to measure the projected interatomic distances in the iDPC-STEM images. The intensity profiles in Figure 1h–j are corresponding to the dash-line frames with the same colors in Figure 1g. And Figure 1h,i indicate the Si-O-Si-2O-Si units between two Si_{10}-rings (red) and on one Si_{10}-ring (blue) respectively, while Figure 1j shows an intensity profile of individual Si-O-Si unit. As we measured, the projected Si–Si distances in the Si-O-Si-2O-Si units are 3.1 and 1.9 Å respectively, consistent with those measured from the structural model. And the intensities of O and 2O atoms also can be identified to confirm the O positions in ZSM-5. Then, we calculated the electrostatic potential of the [010] projection in Figure 1k, which provides a probable simulation for the iDPC-STEM image. As we mentioned above, the intensity in the iDPC-STEM image is nearly proportional to the atomic number Z so that the light O elements can be imaged together with the heavier Si elements with a proper contrast.

Moreover, we acquired the images of ZSM-5 crystal from other typical projections using the iDPC-STEM, and these images further displayed the positions of sinusoidal channels and O bridges inside the framework. From the [100] projection, the sinusoidal channels along *a*-axis of ZSM-5 were clearly imaged in **Figure 2**a. Figure 2b shows the comparison of the iDPC-STEM image, the structural model and the calculated electrostatic potential. The positions of characteristic units with Si/O atoms were identified by the profile analysis in Figure 2c. The imaged structure with defined atomic positions is highly consistent with the given model and simulation (calculated electrostatic potential). These results finely described the unique cross-linked channel system of ZSM-5 along two orthogonal projections ([010] and [100]) to further study the adsorption behaviors inside the framework.

From other three projections, we used the high-resolution images acquired by iDPC-STEM to show its capacity for the light-element imaging. In Figure 2d,e, the atomic arrangement on the (001) surface of ZSM-5 was exhibited with the consistent model and calculation. More importantly, the block units (Si-O islands) in the iDPC-STEM images are bridged by only the O atoms. Although the contrast is relatively low, these 4 separated O bridges are detectable in the profile analysis (Figure 2f). After checking the ZSM-5 structural model, we found that

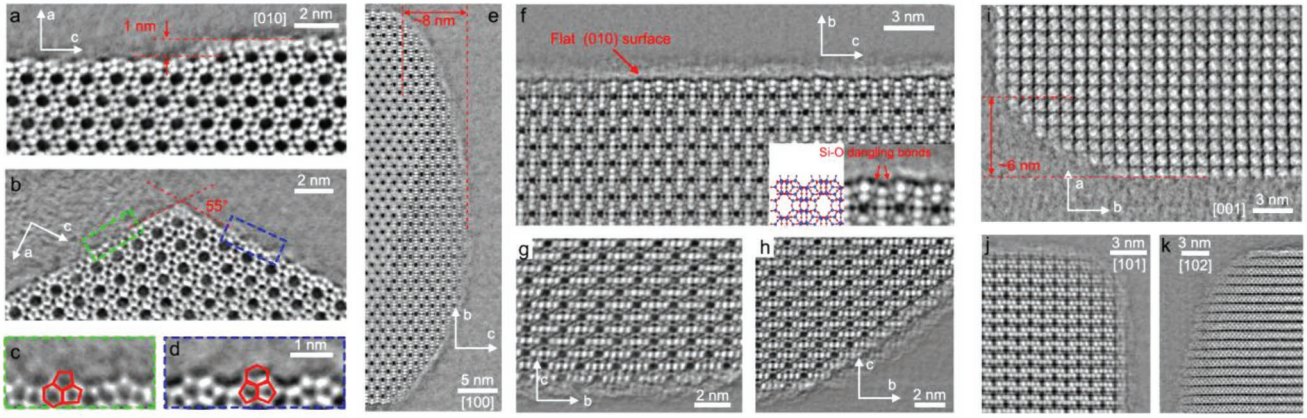

Figure 3. The 3D iDPC-STEM imaging of the surface terminations in ZSM-5. a–d) The iDPC-STEM images of the surface terminations from the [010] projection. c,d) It exhibit the atomic-resolution terminations on the two sides of a crystal corner. e–h) The iDPC-STEM images of the surface terminations from the [100] projection. f) It exhibits the atomically flat (010) surface with clear Si—O dangling bonds. i–k) The iDPC-STEM images of the surface terminations from other three projections, including [001], [101], and [102] respectively.

the [105] and [102] projections provide the better views for the imaging of O bridges as shown in Figure 2g–l. The intensity profiles in Figure 2i,l clearly show the positions of O atoms and their different contrasts compared to the Si–O islands. Moreover, the imaging results from another [101] direction in Figure S4 (Supporting Information) also show the proper contrasts for O element. These results exhibit the excellent capacity of iDPC technique for the light-element imaging.

Based on the atomic-resolution 3D observations of ZSM-5 framework, we could obtain new understandings on the local structures of these short-*b*-axis ZSM-5 nanocrystals, including the terminations of different surfaces and the interfaces in assemblies. First, **Figure 3**a–c shows the lateral surface structures terminated by the halves of Si_{10}-rings from the [010] projection. The termination of (100) surface (Figure 3a) indicated that the ZSM-5 crystals grew layer by layer of half-unit-cell thickness (≈1 nm). And, on the two sides of a corner (marked in Figure 3b), the detailed terminations in Figure 3c,d show the atomic-resolution surface structures, where the Si_5- and Si_6-rings were cut in half as marked respectively. Then, Figure 3e–h exhibit the surface terminations viewed from the [100] projection. Except an 8 nm long area at the edges, the (010) surface maintained atomically flat lasting for several hundred nanometers and was terminated by clear Si/O dangling bonds as shown in Figure 3f inset. And Figure 3i–k provides the results of other typical projections to describe the complete morphology of ZSM-5 nanocrystals. In all these images, the uniform edges in ZSM-5 crystals were formed by the complete or half of unit cells as the energetically preferred terminations. These observations will help us to better understand the synthesis and control of zeolite crystal structures.

To investigate the interfaces between assemblies, we imaged the lateral [100] projection of several ZSM-5 particles stacked from the *b*-axis (**Figure 4**a). The (010) surfaces of these particles

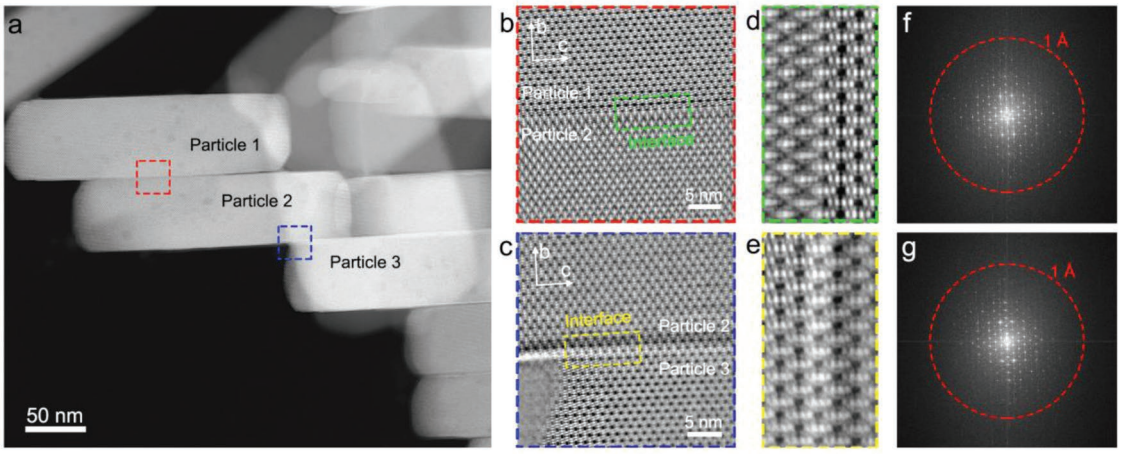

Figure 4. The iDPC-STEM imaging of the (010) interfaces between ZSM-5 particles. a) The HAADF-STEM image of assembled ZSM-5 particles. These particles were stacked from the [010] direction, and their flat (010) surfaces were in close contact with each other. b,c) The iDPC-STEM images of the (010) interfaces in the areas marked in (a). d,e) The zoom-in interface areas of iDPC-STEM images marked in (b,c). f,g) The FFT patterns corresponding to (b) f) and (c) g) respectively. The FFT pattern of adjacent particles shows single set of diffraction spots indicating the coherent alignment of ZSM-5 lattices by the interactions between these (010) surfaces.

were closely connected by the van der Waals interactions. As shown in Figure 4b,c, the adjacent particles showed coherent [010] zone axes so that the sinusoidal channels of two particles can be clearly imaged in one image and the corresponding FFT patterns in Figure 4f,g respectively exhibit the single-crystal-like nature with discrete diffraction spots. Thus, these adjacent particles were coherently aligned by the interactions between them. As shown in the magnified images of (010) interfaces (Figure 4d,e), the lattices passing through these interfaces were perfectly matched and combined without visible gaps. And two particles showed the different defocuses due to the out-plane dislocations (that is, the different thicknesses). Such assembly occurred frequently in these nanocrystals, which increased the transfer distance of hydrocarbons along the b-axis and should be avoided by the surface modification during the catalyst synthesis.

Achieving a high-contrast imaging of light elements by the iDPC technique will not only help us to study the channel geometry and the local structures of such Si-O-based zeolites, but also provide an efficient tool to image and investigate the small molecules mainly consisting of light C, H, and O elements in the hydrocarbon pools directly by the STEM. Here, we filled the ZSM-5 frameworks with PXs as the artificial hydrocarbon pools (see details in "Materials and Methods" section in the Supporting Information) and study their sorption behaviors in ZSM-5 framework. This method provides an ideal model to investigate the hydrocarbon pools by eliminating the complexity due to the multicomponents of the real hydrocarbon pools. The sorption studies have shown that the size-matched PXs will be arranged coherently along the ZSM-5 straight channels due to the strong confinement of frameworks which is related to the channel geometry.[20–22] Thus, the overlapping contrast of PX array in one channel was enhanced to be comparable with that of Si frameworks so that we may observe these small molecules from the [010] projection.

As we expected, **Figure 5**a exhibits the real-space imaging of PXs confined in the straight channels of ZSM-5, and Figure 5b gives the comparison between the 1) iDPC-STEM image, 2)

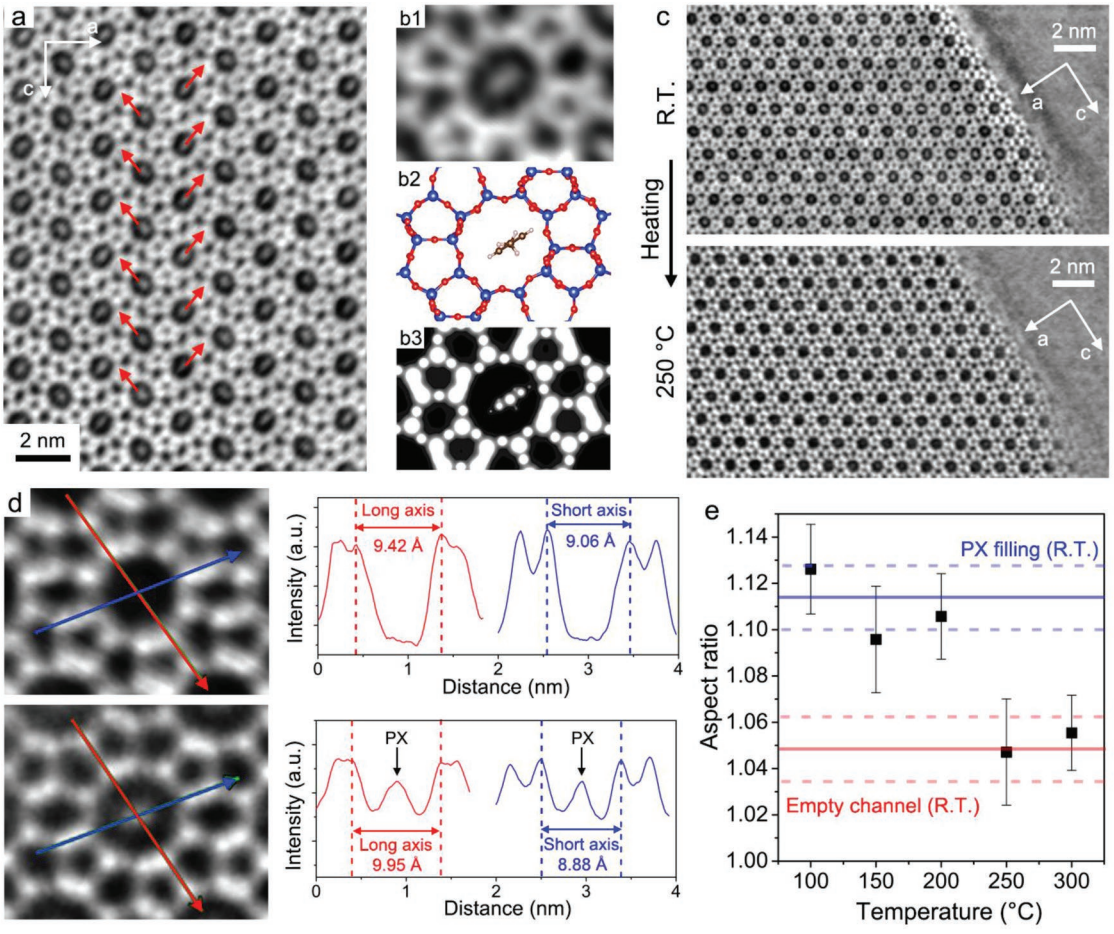

Figure 5. The imaging of PX adsorption in flexible ZSM-5 framework. a) The iDPC-STEM images of the PX-filling ZSM-5 from the [010] projection. b) The corresponding 1) magnified image, 2) calculated structural model, and 3) electrostatic potential of the PX-filling channels. c) The iDPC-STEM images acquired at the same area during the in situ heating process. At over 250 °C, the PXs were desorbed from the ZSM-5 framework. d) The magnified iDPC-STEM images and the intensity profiles of the empty (up) and PX-filling (down) ZSM-5 (arrows marked in images). Here, the long and short axis of straight channel were measured as the distances between the opposite Si atoms in the intensity profiles. e) The change of aspect ratios during the in situ heating process. The blue and red lines show the average values of 1.114 ± 0.014 and 1.048 ± 0.014 in the PX-filling and empty channels. The aspect ratio decreased to the value of empty channels after the PX desorption.

calculated structure, and 3) electrostatic potential. And these imaging results were also obtained by other imaging modes in Figure S5 (Supporting Information). Based on the first-principle calculations (see details in "Materials and Methods" section in the Supporting Information), the PX adsorption at the intersection of the straight and sinusoidal channels is most probable, where the C_6-planes of PXs are nearly parallel to the straight channels. The overlapping projection was imaged as a spindle-shaped spot oriented to the long axis of elliptical Si_{10}-ring (marked as the red arrows in Figure 5a), which was also confirmed by the profile analysis of PX-filling ZSM-5 specimens in Figure S6 (Supporting Information) compared to the results of empty ZSM-5 specimens in Figures S7 and S8 (Supporting Information). Meanwhile, the desorption of PXs can also be imaged after an in situ heating process from the room temperature (R.T.) to over 250 °C (as shown in Figures S9 and S10 in the Supporting Information). In Figure 5c, we observed that the PX spots in channels disappeared from the straight channels in the iDPC-STEM images acquired at the same area during the in situ heating process. These results are consistent with the desorption properties of PXs studied by the thermogravimetry (Figure S11, Supporting Information).

Along with the PX adsorption/desorption, the channel geometry will also change due to the host-guest interactions. It has been confirmed by many ^{29}Si MAS-NMR and XRD results that the straight channels could be deformed by guest molecules,[21,43,44] and such deformation was reversible during the adsorption/desorption process. Using the iDPC-STEM, a series of images at different temperatures can be obtained at the same area without electron beam damage on framework (Figure S9, Supporting Information). Thus, the temporal changes of ZSM-5 framework during the in situ heating were directly imaged here. As shown in Figure 5d, the magnified images and corresponding profile analysis of empty (up) and PX-filling (down) channels were used to measure the deformation of channel geometry. Here the long axis and short axis of straight channel are defined as the distances of opposite Si atoms as marked in Figure 5d (since the Si positions are clearer than the O positions in the intensity profiles). In the profiles of empty channel, the lengths of the long axis and short axis are closer (9.42 and 9.06 Å respectively), while, in the profiles of the PX-filling channel, we can observe the PX intensity peaks in the valleys and the channel was lengthened obviously along the long axis. Then, we used the aspect ratio (defined as the ratio of the long axis to the short axis) to describe the channel geometry, and measured the average aspect ratio at different temperatures (Figure 5e). At R.T. to 200 °C, the values maintained ≈1.11, while, at over 250 °C, the PXs were desorbed from ZSM-5 and the values decreased back to ≈1.05, as same as the average value of empty channels.

Meanwhile, in the images from the [100] projection (Figure S12, Supporting Information), we hardly observed any detectable species and change of channel geometry in the sinusoidal channels after the PX adsorption. As we have calculated, the energy difference between two configurations (in the intersections and channels respectively, Figures S13 and 14 in the Supporting Information) is over 20 kJ mol^{-1}, corresponding to a 3000-fold-higher possibility of the PX adsorption at the intersections. These results visually revealed the preferential PX adsorption sites at the intersections of ZSM-5 channels. Since the channel geometry can be tuned by the guest molecules, these observations provide a new perspective to evaluate the host-guest interactions and design the channel geometry according to the application requirements. To the best of our knowledge, it is the first time that we can observe small aromatics and study their behaviors under any (S)TEMs after substantially reducing the electron beam current.

In summary, we established a strategy to achieve the nearly nondestructive imaging of the ZSM-5 framework and the adsorbed PXs as artificial hydrocarbon pools under ultralow beam current. Based on the iDPC-STEM, we unraveled the local structures of ZSM-5 with the high-contrast imaging of light O elements, and we also revealed the temporal changes of channel geometry during the in situ heating experiments. Then, we investigated the single-molecule sorption behaviors of small aromatics directly by the STEM for the first time. At this scale, the accurate position of each atom in the framework is highly desired to confirm its detailed structure and channel geometry, since the adsorbed PXs will orient along the long axis of elliptical Si_{10}-ring preferentially and induce the slight reversible channel deformation as we observed under the iDPC-STEM. These results help us to understand the surface terminations and interfaces of nanosized ZSM-5 catalysts and investigate the host-guest interactions in the frameworks, which are of great significance to study the physical and chemical properties of reactants and products during diverse catalytic reactions. Moreover, other small molecules can also be imaged and analyzed based on the similar strategy when confined in the matched frameworks, and the iDPC-STEM will show the wide applications to atomically characterize the beam-sensitive catalysts and light-element species that was previously impossible.

Supporting Information

Supporting Information is available from the Wiley Online Library or from the author.

Acknowledgements

This work was supported by the National Basic Research Program of China (973 Program, 2011CB932602) and the National Natural Science Foundation of China (Nos. 20141301065, 21306103, 21771029, and 21573034).

Conflict of Interest

The authors declare no conflict of interest.

Keywords

iDPC-STEM imaging, light-element imaging, para-xylenes, ultra-low beam current, ZSM-5 frameworks

Received: September 17, 2019
Revised: November 9, 2019
Published online: November 29, 2019

[1] H. Li, M. Eddaoudi, M. O'Keeffe, O. M. Yaghi, *Nature* **1999**, *402*, 276.
[2] H. Furukawa, K. E. Cordova, M. O'Keeffe, O. M. Yaghi, *Science* **2013**, *341*, 1230444.
[3] A. P. Côté, A. I. Benin, N. W. Ockwig, M. O'Keeffe, A. J. Matzger, O. M. Yaghi, *Science* **2005**, *310*, 1166.
[4] C. S. Diercks, O. M. Yaghi, *Science* **2017**, *355*, eaal1585.
[5] C. S. Cundy, P. A. Cox, *Chem. Rev.* **2003**, *103*, 663.
[6] Y. Li, J. Yu, *Chem. Rev.* **2014**, *114*, 7268.
[7] W. J. Roth, P. Nachtigall, R. E. Morris, J. Čejka, *Chem. Rev.* **2014**, *114*, 4807.
[8] E. M. Flanigen, J. M. Bennett, R. W. Grose, J. P. Cohen, R. L. Patton, R. M. Kirchner, J. V. Smith, *Nature* **1978**, *271*, 512.
[9] G. T. Kokotailo, S. L. Lawton, D. H. Olson, W. M. Meier, *Nature* **1978**, *272*, 437.
[10] M. Bjørgen, S. Svelleb, F. Joensena, J. Nerlova, S. Kolboeb, F. Boninoc, L. Palumboc, S. Bordigac, U. Olsbyeb, *J. Catal.* **2007**, *249*, 195.
[11] D. Lesthaeghe, J. van der Mynsbrugge, M. Vandichel, M. Waroquier, V. van Speybroeck, *ChemCatChem* **2011**, *3*, 208.
[12] S. Ilias, A. Bhan, *ACS Catal.* **2013**, *3*, 18.
[13] Y. Ma, D. Cai, Y. Li, N. Wang, U. Muhammad, A. Carlsson, D. Tang, W. Qian, Y. Wang, D. Su, F. Wei, *RSC Adv.* **2016**, *6*, 74797.
[14] Y. Ma, N. Wang, W. Qian, Y. Wang, J. Zhang, F. Wei, *RSC Adv.* **2016**, *6*, 81198.
[15] C. Zhang, R. P. Lively, K. Zhang, J. R. Johnson, W. J. Koros, *J. Phys. Chem. Lett.* **2012**, *3*, 2130.
[16] R. V. Awati, P. I. Ravikovitch, D. S. Sholl, *J. Phys. Chem. C* **2013**, *117*, 13462.
[17] S. Boulfelfel, P. I. Ravikovitch, D. S. Sholl, *J. Phys. Chem. C* **2015**, *119*, 15643.
[18] R. J. Verploegh, S. Nair, D. S. Sholl, *J. Am. Chem. Soc.* **2015**, *137*, 15760.
[19] P. J. Bereciartua, Á. Cantín, A. Corma, J. L. Jordá, M. Palomino, F. Rey, S. Valencia, E. W. Corcoran Jr., P. Kortunov, P. I. Ravikovitch, A. Burton, C. Yoon, Y. Wang, C. Paur, J. Guzman, A. R. Bishop, G. L. Casty, *Science* **2017**, *358*, 1068.
[20] D. H. Olson, G. T. Kokotailo, S. L. Lawton, W. M. Meier, *J. Phys. Chem.* **1981**, *85*, 2238.
[21] R. Goyal, A. N. Fitch, H. Jobic, *J. Phys. Chem. B* **2000**, *104*, 2878.
[22] C. A. Fyfe, J. S. J. Lee, L. M. D. Cranswick, I. Swainson, *Microporous Mesoporous Mater.* **2008**, *112*, 299.
[23] J. M. Cowley, *Ultramicroscopy* **1976**, *2*, 3.
[24] M. Haider, S. Uhlemann, E. Schwan, H. Rose, B. Kabius, K. Urban, *Nature* **1998**, *392*, 768.
[25] R. Erni, M. D. Rossell, C. D. Kisielowski, U. D. Dahmen, *Phys. Rev. Lett.* **2009**, *102*, 96.
[26] Y. Sasaki, T. Suzuki, Y. Takamura, A. Saji, H. Saka, *J. Catal.* **1998**, *178*, 94.
[27] O. I. Lebedev, F. Millange, C. Serre, G. van Tendeloo, G. Ferey, *Chem. Mater.* **2005**, *17*, 6525.
[28] C. Baerlocher, F. Gramm, L. Massüger, L. B. McCusker, Z. He, S. Hovmöller, X. Zou, *Science* **2007**, *315*, 1113.
[29] J. Cravillon, S. Münzer, S. J. Lohmeier, A. Feldhoff, K. Huber, M. Wiebcke, *Chem. Mater.* **2009**, *21*, 1410.
[30] A. Mayoral, T. Carey, P. A. Anderson, A. Lubk, I. Diaz, *Angew. Chem., Int. Ed.* **2011**, *50*, 11230.
[31] T. Willhammar, J. Sun, W. Wan, P. Oleynikov, D. Zhang, X. Zou, M. Moliner, J. Gonzalez, C. Martinez, F. Rey, A. Corma, *Nat. Chem.* **2012**, *4*, 188.
[32] L. K. Zhu, D. L. Zhang, M. Xue, H. Li, S. L. Qiu, *CrystEngComm* **2013**, *15*, 9356.
[33] T. Willhammar, A. Mayoral, X. Zou, *Dalton Trans.* **2014**, *43*, 14158.
[34] S. Smeets, D. Xie, C. Baerlocher, L. B. McCusker, W. Wan, X. Zou, S. I. Zones, *Angew. Chem.* **2014**, *126*, 10566.
[35] A. Mayoral, R. Mahugo, M. Sanchez-Sanchez, I. Diaz, *ChemCatChem* **2017**, *9*, 3497.
[36] Y. Zhu, J. Ciston, B. Zheng, X. Miao, C. Czarnik, Y. Pan, R. Sougrat, Z. Lai, C.-E. Hsiung, K. Yao, I. Pinnau, M. Pan, Y. Han, *Nat. Mater.* **2017**, *16*, 532.
[37] D. Zhang, Y. Zhu, L. Liu, X. Ying, C.-E. Hsiung, R. Sougrat, K. Li, Y. Han, *Science* **2018**, *359*, 675.
[38] W. Wan, J. Su, X. Zou, T. Willhammar, *Inorg. Chem. Front.* **2018**, *5*, 2836.
[39] H. Rose, *Ultramicroscopy* **1976**, *2*, 251.
[40] S. Majert, H. Kohl, *Ultramicroscopy* **2015**, *148*, 81.
[41] I. Lazic, E. G. T. Bosch, S. Lazar, *Ultramicroscopy* **2016**, *160*, 265.
[42] E. Yucelen, I. Lazic, E. G. T. Bosch, *Sci. Rep.* **2018**, *8*, 2676.
[43] C. A. Fyfe, G. J. Kennedy, C. T. De Schutter, G. T. Kokotailo, *J. Chem. Soc., Chem. Commun.* **1984**, *8*, 541.
[44] C. A. Fyfe, H. Strobl, G. T. Kokotailo, G. J. Kennedy, G. E. Barlow, *J. Am. Chem. Soc.* **1988**, *110*, 3373.